



1 **Roles of electrons and ions in formation of the current in**
2 **mirror mode structures in the terrestrial plasma sheet:**
3 **MMS observations**

4 Guoqiang Wang^{1,2}, Tielong Zhang^{1,3}, Mingyu Wu¹, Daniel Schmid¹, Yufei Hao⁴,
5 Martin Volwerk³

6 ¹Institute of Space Science and Applied Technology, Harbin Institute of Technology, Shenzhen,
7 China
8 ²Key Laboratory of Lunar and Deep Space Exploration, Chinese Academy of Sciences, Beijing,
9 China
10 ³Space Research Institute, Austrian Academy of Sciences, Graz, Austria
11 ⁴Key Laboratory of Planetary Sciences, Purple Mountain Observatory, Chinese Academy of
12 Sciences, Nanjing, China

13
14 **Abstract**

15 Currents are believed to exist in mirror mode structures and to be self-consistent with
16 the magnetic field depression. Here, we investigate a train of mirror mode structures in
17 the terrestrial plasma sheet on 11 August 2017 measured by the Magnetospheric
18 Multiscale mission data. We find that a bipolar current exists in the cross-section of two
19 hole-like mirror mode structures, referred to as magnetic dips. The bipolar current in
20 the magnetic dip with a size of $\sim 3 \rho_i$ (the ion gyro radius) is mainly contributed by an
21 electron bipolar velocity, which is mainly formed by the magnetic gradient-curvature
22 drift. For another magnetic dip with a size of $\sim 6.67 \rho_i$, the bipolar current is mainly
23 caused by an ion bipolar velocity, which can be explained by the ion diamagnetic drift.
24 These observations suggest that the electrons and ions play different roles in the
25 formation of currents in magnetic dips with different sizes.



26 **1 Introduction**

27 Mirror modes are pressure-balanced and compressional magnetic structures
28 (Hasegawa, 1969; Tsurutani et al., 2011; Wang et al., 2016; Zhang et al., 2018). They
29 widely exist in many space plasma regions, such as solar wind (Zhang et al., 2008, 2009;
30 Russell et al., 2009), planetary magnetosheath (Volwerk et al., 2008; Schmid et al.,
31 2014), planetary magnetosphere (Vaivads et al., 2001; Rae et al., 2007), and comets
32 (Glassmeier et al., 1993; Volwerk et al., 2016). These structures are believed to be
33 generated by the mirror instability excited in the mirror unstable environment
34 (Hasegawa, 1969; Southwood and Kivelson, 1993). The plasma perpendicular
35 temperature anisotropy provides free energy to excite the mirror instability (Kivelson
36 and Southwood, 1996). Once the mirror mode structures are generated, they will
37 convected with the ambient flow since they are non-propagating relative to the ambient
38 flow (Tsurutani et al., 2011). It is expected that they will stop to grow or decay when
39 they move to the mirror stable region. Actually, they are reported to be able to survive
40 in the mirror stable region in the solar wind and magnetosheath (Balikhin et al., 2009;
41 Russell et al., 2009).

42

43 Mirror mode structures appears as not only quasi-periodic sinusoidal oscillations, but
44 also local enhancements or decrease of the magnetic field intensity, referred to as
45 magnetic peaks or dips (Tsurutani et al., 2011). Magnetic peaks can only exist in the
46 mirror unstable environments, while magnetic dips are able to survive in the mirror
47 stable region (Kuznetsov et al., 2007; Soucek et al., 2008). The typical scales of the
48 mirror mode structures are $10s \rho_i$ in the magnetosheath (Tsurutani et al., 1982; Horbury
49 and Lucek, 2009), where ρ_i is the ion gyro radius. Based on observations of the four
50 Cluster satellites, the longest scales of the mirror mode structures in the magnetosheath
51 is found to be 2 – 6 times length of their shortest scales, and their shapes are
52 approximately cigar-like (Horbury and Lucek, 2009).

53

54 In the terrestrial plasma sheet, there also exist mirror mode structures with several



55 ion gyro radii (Vaivads et al., 2001; Zieger et al., 2011; Li et al., 2014; Wang et al.,
56 2016). The earthward fast flows can result in a magnetic pileup in its leading area, and
57 the ion perpendicular temperature anisotropy in the pileup region is able to make the
58 local plasma conditions mirror-unstable to generate mirror mode structures (Zieger et
59 al., 2011). Mirror mode structures accompanied by electron dynamics and whistler
60 waves are also reported to occur during the dipolarization processes in the plasma sheet
61 (Li et al., 2014). Dipolarization fronts (DFs), characterized by a sharp enhancement in
62 B_z in GSM, are formed ahead of the earthward fast flows (Ge et al., 2012; Wu et al.,
63 2013; Schmid et al., 2016; Xiao et al., 2017). They create a magnetic pileup region
64 ahead of the DF when moving earthward (Schmid et al., 2011; Fu et al., 2012; Liu et
65 al., 2013). Mirror mode structures with a scale of $\sim 4 \rho_i$ are reported to occur in the
66 magnetic pileup region ahead of a DF, and the mirror instability is suggested to be a
67 potential mechanism to generate these structures since local environments are mirror-
68 unstable (Wang et al., 2016). Within a mirror mode structure there should be an electric
69 current driven by the magnetic gradient and curvature drifts of the ions and/or electrons
70 in order to sustain their stability (Constantinescu, 2002).

71

72 In this study, we investigate a train of mirror mode structures in the terrestrial plasma
73 sheet on 11 August 2017 using the Magnetospheric Multiscale (MMS) mission data.
74 The aim of this study is to figure out the roles of electrons and ions in the current inside
75 the mirror mode structure based on the high-resolution MMS data.

76

77 **2 Observation**

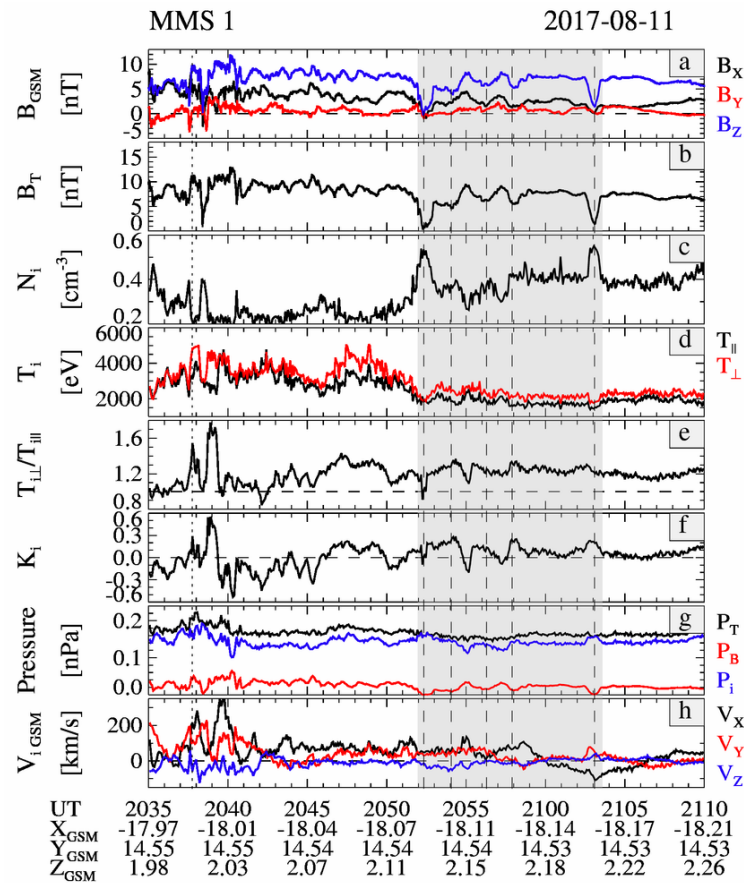
78 The MMS spacecraft consist of four identical satellites, which constitute a
79 tetrahedron with inter-spacecraft distances of tens km (Burch et al., 2015). In the
80 present study, we use the survey (a resolution of 16 Hz) and burst (128 Hz) magnetic
81 field data obtained by the Fluxgate Magnetometer (Russell et al., 2014), and the survey
82 (4.5 s) and burst (150 ms for ions, 30 ms for electrons) plasma data recorded by the Fast
83 Plasma Instrument (Pollock et al., 2016). Since the burst magnetic and plasma data are



84 only available in parts of the interval in Figure 1, the survey data are used throughout
85 the paper unless stated otherwise.

86

87 Figure 1 shows that B_z sharply increases ~ 8 nT within 7 seconds at $\sim 20:38$ UT on 11
88 August 2017 accompanied by a fast earthward flow with a maximum velocity ~ 300
89 km/s. Also, the local ion beta, the ratio of the ion thermal pressure to the magnetic
90 pressure is ~ 4 , and the elevation angle ($\theta = \arctan\left(\frac{B_z}{\sqrt{B_x^2 + B_y^2}}\right)$) changes $\sim 50^\circ$ with a
91 maximum angle of 64° (not shown). These observations satisfy the criteria of the DF
92 from Fu et al. (2012), indicating that it is a DF event shown as the vertical dotted line
93 in Figure 1. At 20:40 UT, the MMS spacecraft are located near $(-18, 14.6, 2)$ R_E in
94 GSM (Geocentric Solar Magnetospheric coordinates, used everywhere unless
95 otherwise stated). The normal direction of the DF is $(0.34, 0.82, -0.46)$ determined by
96 the minimum variance analysis (MVA) (Sonnerup and Scheible, 1998) using the data
97 in the interval between 20:37:33 and 20:37:42 UT. The ratio of the intermediate to
98 minimum eigenvalues (λ_2/λ_3) is ~ 15 , indicating that the estimated normal direction is
99 reliable (Volwerk, 2006; Wang et al., 2014). The estimated normal direction suggests
100 that the MMS spacecraft are located at the duskward side of the DF based on the semi-
101 circle assumption of the DF (Huang et al., 2015).



102
 103 **Figure 1.** Observations of a DF event by MMS 1 on 11 August 2017. From top to bottom: three
 104 components of the magnetic field in GSM (a), the total magnetic field (b), ion density (c), ion
 105 perpendicular (red) and parallel (black) temperatures (d), ion perpendicular temperature anisotropy
 106 (e), the threshold of the mirror instability (f), the magnetic, ion thermal and total pressures (g), and
 107 three components of the ion velocity in GSM (h). The vertical dotted line indicates the DF, and the
 108 dashed lines indicates the trough of each compressional structure. The gray shadows indicate the
 109 mirror mode structures.

110
 111 Several quasi-periodic compressional magnetic oscillations with a period of ~ 2 min
 112 are observed in the interval between 20:51 and 21:04 UT shown as the gray region in
 113 Figure 1. Since waves with a period of ~ 20 s are superimposed on the compressional
 114 oscillations, and only burst magnetic field data are available before 20:53 UT for this
 115 interval, we estimate the velocities of these compressional oscillations by timing



116 analysis (Harvey, 1998) using the burst magnetic field data low-pass filtered with a
117 cutoff period of 30 s between 20:51:55 and 20:53 UT. The estimated velocity is (61.6,
118 12.7, -33.5) km/s, which is close to the average ion velocity (49.3, 38.2, -35.2) km/s in
119 this interval, suggesting that these oscillations are approximately stationary in the
120 ambient flow. The ion number density tends to be larger in the trough of the oscillations
121 as the dashed lines shown in Figure 1. Figure 1g shows that the magnetic and ion
122 thermal pressures vary in anti-phase during the compressional oscillations, in addition,
123 the total pressure is almost constant, indicating that the oscillations are pressure-
124 balanced. The above properties of the compressional oscillations indicate that they are
125 mirror mode structures (Tsurutani et al., 2011).

126

127 We mark these mirror mode structures as MM1 to MM5, and their time intervals and
128 scales are listed in Table 1. The scales are estimated by

$$129 \quad \sqrt{\left(\int_{t_1}^{t_2} V_X dt\right)^2 + \left(\int_{t_1}^{t_2} V_Y dt\right)^2 + \left(\int_{t_1}^{t_2} V_Z dt\right)^2}$$

130 where V_X , V_Y and V_Z are three components of the ion velocity, while t_1 and t_2 are the
131 start and end time of each structure (Ge et al., 2011). And the local ion gyro radius ρ_i is
132 estimated by the average ion temperature and average total magnetic field low-pass
133 filtered with a cutoff period of 20 s. The scales of these structures vary between $\sim 3 \rho_i$
134 and $14.38 \rho_i$. The rotation angle of the magnetic field over each structure varies between
135 $\sim 2.5^\circ$ and 12.4° .

136

137 The threshold of the ion mirror instability K_i is shown in Figure 1f, where $K = \frac{T_\perp}{T_\parallel} -$
138 $1 - \frac{1}{\beta_\perp}$, and T_\perp , T_\parallel , and β_\perp are perpendicular and parallel ion temperatures and
139 perpendicular ion beta, respectively (Southwood, and Kivelson, 1993). Local plasma
140 environments become mirror unstable and can excite ion mirror instabilities when $K_i >$
141 0. The maximum K_i in each mirror mode structure reaches over 0.2, and it tends to
142 decrease to near or below 0 from the center of each structure to its edge. Before 20:51



143 UT or after 21:04 UT, K_i is near or below 0, i.e. the background environment for these
144 structures is mirror marginal stable.

145

Table 1. The time interval, angle of the magnetic field at two edges, scale, and maxima threshold of the ion mirror instability for each mirror mode structure.

	Time interval (HH:MM:SS)	θ (°)	ρ_i	Scale (km)	K_{i_max}
MM1	20:51:55 – 20:53:06 UT	13.3	3	4.83×10^3	0.2
MM2	20:53:06 – 20:55:00 UT	6.3	14.41	11.32×10^3	0.28
MM3	20:55:00 – 20:57:14 UT	4.6	12.36	8.25×10^3	0.17
MM4	20:57:14 – 20:58:56 UT	6.3	12.93	8.39×10^3	0.25
MM5	21:02:26 – 21:03:34 UT	2.9	6.67	6.42×10^3	0.23

146

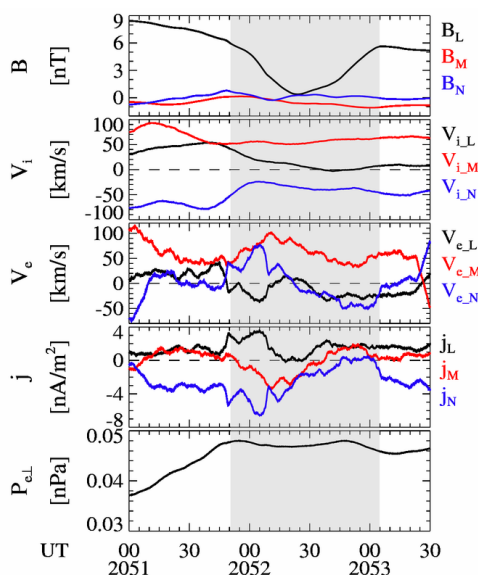
147 MM1 and MM5 appear as hole-like structure, which are referred to as magnetic dips
148 (Tsurutani et al., 2011). To further look at the plasma properties in the magnetic dips,
149 we transform the ion and electron velocities as well as the magnetic field and current
150 density into the principal axis (LMN) coordinate system. The principal axes vectors are
151 calculated by the minimum variance analysis (MVA, Sonnerup and Scheible, 1998) in
152 the interval between 20:51:55 and 20:53:06 UT. The \mathbf{L} , \mathbf{M} and \mathbf{N} directions are (0.44,
153 0.17, 0.88), (0.33, 0.88, -0.34) and (-0.84, 0.44, 0.33) in GSM, respectively. The ratio
154 of the intermediate to minimum eigenvalues is ~ 4.7 , indicating that the MVA results are
155 reliable (Sergeev et al., 2003). The current density is calculated by $\mathbf{j} = qn_e(\mathbf{V}_i - \mathbf{V}_e)$,
156 where n_e , \mathbf{V}_i , and \mathbf{V}_e are electron number density, ion velocity and electron velocity,
157 respectively. To reduce the effect of the high-frequency oscillations, the magnetic field,
158 electron velocity and current density in Figure 2 (also in Figure 3) have been smoothed
159 within a 20-second window.

160

161 Figure 2 shows that B_L is dominant while B_M and B_N vary around 0, indicating that
162 the cross-section of the structure is approximately parallel to the M-N plane. The ion
163 velocity is mainly in the M-N plane during the whole interval, and there are no
164 significant changes in both V_{i_M} and V_{i_N} . By contrast, the N component of the electron
165 velocity V_{e_N} shows a bipolar variation with a maximum change of ~ 70 km/s. An
166 enhancement (a decrease) of V_{e_N} occurs in the left (right) side of MM1. One can also



167 note that the maximum and minimum of V_{e_N} in MM1 tend to occur near the maximum
 168 gradient of B_L . V_{e_M} also shows a bipolar variation in MM1 compared to the ambient
 169 value. In addition, the N and M components of the current density show bipolar
 170 variations similar to the electron velocity with an opposite trend of change. By
 171 comparing the variations in the ion and electron velocities, one can note that the current
 172 density in MM1 is mainly determined by the the electron velocity. The bottom panel in
 173 Figure 2 shows the electron perpendicular thermal pressure $P_{e\perp}$, and there is no
 174 significant change in $P_{e\perp}$ in MM1.
 175

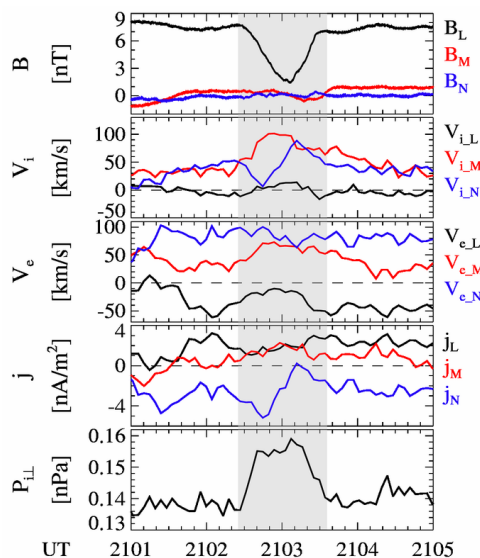


176
 177 **Figure 2.** Three components of the magnetic field, ion and electron velocities, current density in the
 178 principal axis (LMN) coordinate system, and electron perpendicular thermal pressure between 20:51
 179 and 20:53:30 UT.

180
 181 Figure 3 shows the magnetic field, ion velocity, electron velocity, current density and
 182 ion perpendicular thermal pressure in MM5. The magnetic field data between 21:02:30
 183 and 21:03:30 UT are used to calculate the principal axes vectors by MVA (Sonnerup
 184 and Scheible, 1998). The ratio of the intermediate to minimum eigenvalues is ~ 6.8 , and
 185 the **L**, **M** and **N** directions are $(0.26, 0.09, 0.96)$, $(-0.49, 0.87, 0.05)$ and $(-0.83, -0.49,$



186 0.27) in GSM, respectively. B_L is dominant during the whole interval, while B_M and B_N
 187 are very small. Thus, the cross-section of MM5 is approximately parallel to the M-N
 188 plane. The ion velocity V_{i_M} and V_{i_N} are dominant, while V_{i_L} varies around 0.
 189 Interestingly, a bipolar feature in V_{i_N} with a variation up to 73 km/s (peak minus trough)
 190 can be distinctly found in the dip, while V_{i_M} tends to increase compared to the ambient
 191 flow. V_{i_N} is smaller (larger) than the ambient value in the left (right) side of the dip. J_N
 192 also shows a similar bipolar feature with a variation up to 5.4 nA/m², while J_L and J_N
 193 have no significant changes. The N component of the electron velocity, however, shows
 194 no such characteristics, indicating that the bipolar J_N is mainly determined by the
 195 bipolar V_{i_N} . The ion perpendicular thermal pressure $P_{i\perp}$ in the structure is obviously
 196 larger than the ambient value, and $P_{i\perp}$ tends to be larger from the edge to the center of
 197 MM5.



198
 199 **Figure 3.** Three components of the magnetic field, ion and electron velocities, current density in the
 200 principal axis (LMN) coordinate system, and ion perpendicular thermal pressure between 2101 and
 201 2105 UT.

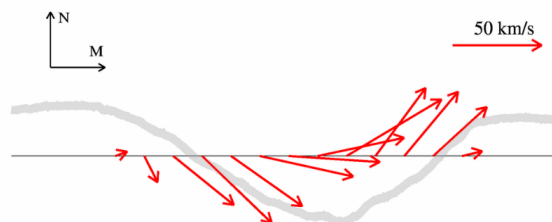
202

203 To look at the variations of the ion flow in MM5, we assume that the ion velocity
 204 observed during MM5 consists of V_{i_a} and $V_{i_{md}}$, where V_{i_a} is the ambient ion velocity,
 205 and $V_{i_{md}}$ is the ion velocity in the magnetic dip relative to the ambient flow. The



206 average velocity 30 seconds before and after MM5 is selected to be regarded as V_{i_a}
207 with a value of (-2.6, 51.4, 33.4) km/s in LMN. Figure 4 shows the deflection of $V_{i_{md}}$
208 in the M-N plane. The arrows indicate the direction of the ion velocity, and their lengths
209 indicate the magnitude of $V_{i_{md}}$ in the M-N plane. The direction of $V_{i_{md}}$ gradually
210 changes from around -60° to 50° in the M-N plane. Also, the strength of $V_{i_{md}}$ in this
211 plane gradually increases and then decreases from the left side of the magnetic dip to
212 the right side. In addition, the N component of $V_{i_{md}}$ changes from negative to positive
213 at just around the center of the structure.

214



215

216 **Figure 4.** Ion velocities in the M-N plane during MM5. The arrows indicates the direction of the
217 ion velocities, and their lengths indicate the amplitude of the ion velocities. And the gray line
218 indicates the total magnetic field of MM5.

219

220 3 Discussion

221 Figure 1 shows the ambient plasma is marginally mirror stable, indicating that the
222 mirror mode structures are not locally generated. Since they are stationary in the
223 ambient flow, they are estimated to occur dawnside of the MMS spacecraft with a
224 distance of $\sim 4 R_E$ in the Y direction when the spacecraft are crossing the DF at around
225 20:38 UT, where the average $V_Y \sim 30$ km/s during the structures are used. Compared
226 this distance with the typical size of the DF ($\sim 3 R_E$) (Huang et al., 2015) and the size of
227 the structures, the mirror mode structures might come from the dawnside flank of the
228 DF. Since the DF is considered to be a tangential discontinuity (Schmid et al., 2019)
229 which pushes the background plasma to its flanks (Fu et al., 2012; Liu et al., 2013), the
230 plasma near the flank is expected to come from the pileup region ahead of DFs. Mirror



231 mode structures have been reported to occur in such a pileup region (Wang et al., 2016).
232 The pileup of the magnetic field and the ion reflection ahead of the DF are suggested
233 to provide free energy to excite the ion mirror instability (Zieger et al., 2011; Wang et
234 al., 2016). Thus, the mirror mode structures in Figure 1 might originate from the pileup
235 region ahead of the DF.

236

237 Based on Ampère's law, there should exist a current in the magnetic dip to sustain
238 the structure's stability, and the current is determined by the collective behavior of
239 electrons and ions (see Constantinescu, 2002). Figure 2 and 3 shows that a bipolar
240 current density is observed in both MM1 and MM5. B_L changes ~ 6 nT in MM1, and
241 the estimated length of MM1 is 4.83×10^3 km. Thus, a current density j_B with a value
242 of ~ 2 nA/m² is necessary to be self-consistent with the magnetic field depression. The
243 amplitude of the bipolar j_N in MM1 is ~ 2 nA/m², almost equal to j_B , indicating that
244 MM1 is a stable structure (Constantinescu, 2002). Similarly, MM5 is also a stable
245 structure. The variations of the current density in MM1 is mainly contributed by the
246 variations of the electron velocity. By contrast, no significant changes occur in the
247 electron velocity, while a bipolar ion velocity similar to the current density appears in
248 V_{iN} . Thus, the bipolar current density in MM5 is mainly contributed by the variations
249 of the ion velocity.

250

251 The size of MM1 is $\sim 3 \rho_i$, and its central magnetic field strength is almost 0. Thus,
252 the ion gyro radius is expected to significantly change within one orbit, and ions would
253 randomly jump between neighboring magnetic dips (Constantinescu, 2002). These ions
254 are referred to as chaotic particles, which do not contribute to the formation of the
255 current in the mirror mode structure (Constantinescu, 2002). It might be an important
256 reason that the current in MM1 is mainly contributed by electrons. The size of MM1 is
257 $\sim 20 \rho_e$, where ρ_e is the local electron gyro radius. Thus, a quasi-hydrodynamic treatment
258 can be used to describe the electrons. Three kind of drifts are expected to form the
259 current in MM1, i.e. the magnetic gradient drift, the magnetic curvature drift, and the



260 electron diamagnetic drift. The electron perpendicular thermal pressure $P_{e\perp}$ changes
261 ~ 0.002 nPa in MM1, the average electron number density is ~ 0.4 cm⁻³, and the average
262 total magnetic field is ~ 3 nT. Consequently, the estimated electron diamagnetic drift
263 velocity is ~ 4 km/s, much smaller than the bipolar amplitude ~ 70 km/s in V_{e_N} in Figure
264 2. We also calculate the magnetic gradient drift velocity with an estimated value of 1.13
265 $\times 10^2$ km/s, where the electron perpendicular temperature is ~ 800 eV, and B_L changes
266 ~ 6 nT in a length of 2.45×10^2 km. Figure 2 shows that the strength of the bipolar
267 velocity in V_{e_N} is ~ 70 km/s, smaller than the magnetic gradient drift velocity. The
268 magnetic curvature drift in MM1 is in the opposite direction of the magnetic gradient
269 drift. Figuring out the magnetic field geometry, we can get the exact values of the
270 magnetic gradient and curvature drifts. Due to the small interspacecraft distance among
271 the MMS satellites, it is difficult to get a reasonable magnetic field geometry and a
272 reliable curvature radius of MM1. Nevertheless, it is expected that both the magnetic
273 gradient and curvature drifts contribute significantly to the formation of the current in
274 MM1.

275

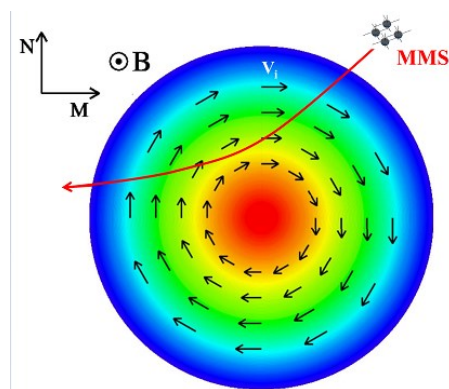
276 The size of MM5 is $\sim 6.67 \rho_i$, larger than that of MM1. The ion bipolar velocity in
277 MM5 indicates a local ion flow, suggesting there exists some magnetohydrodynamic
278 properties in this structure. The ion perpendicular thermal pressure tends to be larger
279 from the edge of MM5 towards its center (see Figure 3), therefore, an ion diamagnetic
280 drift is expected to be formed (Baumjohann and Treumann, 1996). The ion
281 perpendicular thermal pressure changes by ~ 0.013 nPa for intervals 21:02:31 –
282 21:02:40 UT and 21:03:07 – 21:03:29 UT (see Figure 3). Using the average ion density
283 and magnetic field strength, the estimated velocities of the diamagnetic drift are 40.4
284 km/s and 19.2 km/s for these two intervals, which is comparable with the amplitude of
285 the bipolar V_{i_N} in Figure 3. Therefore, the ion bipolar velocity as well as the bipolar
286 current in MM5 is mainly contributed by the ion diamagnetic drift. It is expected that
287 the magnetic gradient and curvature drifts of ions move in opposite directions in MM5.
288 We speculate that the difference of the magnetic gradient and curvature drift velocities



289 are small possibly resulting from the magnetic field geometry of MM5. The larger scale
290 of MM5 compared to MM1 could reduce the magnetic gradient and electron thermal
291 pressure gradient resulting in slower magnetic gradient drift and electron diamagnetic
292 drift velocities. That's could be the reason why no significant bipolar occurs in the
293 electron velocity in MM5. Another possible reason might the magnetic field geometry
294 which might reduce the difference of the magnetic gradient and curvature drift
295 velocities of electrons.

296

297 One can note that there is an enhancement of V_{i_M} in MM5. To figure out the
298 variations of V_{i_M} and V_{i_N} in MM5, we analyze the possible trajectory of the MMS
299 spacecraft crossing MM5. Mirror mode structures in the magnetosheath are found to be
300 cigar-like structures instead of sheets or tubes (Constantinescu et al., 2003; Horbury
301 and Lucek, 2009). To simplify our analysis, we assume that the cross-section of the
302 MM5 structure is a circle. To be self-consistent with the magnetic field depression, the
303 ion flow as well as the current is supposed to be clockwise as the black arrows shown
304 in Figure 5. We calculate the normal directions of the two sides of the magnetic dip by
305 MVA, and the values are (0.03, 0.79, 0.61) and (-0.05, -0.65, 0.76) in LMN for the
306 intervals 21:02:30 – 21:03 and 21:03:10 – 21:03:25 UT, respectively. The ratios of the
307 intermediate to minimum eigenvalues λ_2/λ_3 are 6.4 and 8.5, respectively. Thus, we can
308 get a possible trajectory of MMS in the M-N plane based on the ambient flow and the
309 above normal directions as the red arrow shown in Figure 5. Along the trajectory, one
310 can note that the N component of the ion velocity changes from negative to positive
311 from one to another side of MM5, while the M component is positive, which is in
312 agreement with the deflection of the ion flow shown in Figure 4. Thus, the variations
313 of V_{i_M} and V_{i_N} indicates a ring-like flow in the cross-section of MM5. Such a ring-
314 like flow might play an important role in the evolution of the mirror mode structure or
315 maintaining the stability of the magnetic dip.



316
317 **Figure 5.** Schematic of MMS crossing the magnetic dip in the M-N plane. The colors changing
318 from center (red) of the magnetic dip to its edge (blue) indicate the decrease of the ion perpendicular
319 thermal pressure. The back arrows in the magnetic dip indicate the direction of the ion velocity. The
320 red arrow indicates a possible trajectory of MMS.

321

322 **4 Summary**

323 We have studied the mirror mode structures with a size of several to $14.41 \rho_i$ in the
324 plasma sheet on 11 August 2017. Current is expected to exist in the magnetic dip
325 contributed by the collective behavior of electrons and ions. Our observations show a
326 bipolar current in two magnetic dipoles, and the electrons and ions play different roles in
327 each dip. The bipolar current in the magnetic dip with a size of $\sim 3 \rho_i$ is mainly
328 contributed by an electron bipolar velocity. The bipolar electron velocity could mainly
329 result from the magnetic and curvature drifts of electrons. The chaotic motion of ions
330 might be one significant reason that ions have almost no contribution to the formation
331 of the current in this magnetic dip. For another magnetic dip with a size of $6.67 \rho_i$, the
332 bipolar current is mainly contributed by the ion bipolar velocity, which can be explained
333 by the ion diamagnetic drift velocity. We suggest that both the scale and magnetic
334 geometry of magnetic dipoles are significant to determine the roles of electrons and ions
335 in the formation of the current in dipoles.



336 References

- 337 Balikhin, M. A., Sagdeev, R. Z., Walker, S. N., Pokhotelov, O. A., Sibeck, D. G., Beloff,
338 N., and Dudnikova, G., THEMIS observations of mirror structures: Magnetic holes
339 and instability threshold, *Geophys. Res. Lett.*, 36,
340 <https://doi.org/10.1029/2008GL036923>, 2009.
- 341 Baumjohann, W., and Treumann, R. A., *Basic Space Plasma Physics*, Imperial Coll.
342 Press, London, pp. 147-149, 1997.
- 343 Burch, J. L., Moore, T. E., Torbert, R. B., and Giles, B. L., Magnetospheric multiscale
344 overview and science objectives, *Space Sci. Rev.*, 199, 5–21, 2015.
- 345 Constantinescu, O. D., Self-consistent model for mirror structures, *J. Atmos. Sol. Terr.*
346 *Phys.*, 64, 645–649, 2002.
- 347 Constantinescu, O. D., K.-H. Glassmeier, R. Treumann, and K.-H. Fornacon, Magnetic
348 mirror structures observed by Cluster in the magnetosheath, *Geophys. Res. Lett.*, 30,
349 4–1, 2003.
- 350 Fu, H. S., Khotyaintsev, Y. V., Vaivads, A., André, M., and Huang, S. Y., Occurrence
351 rate of earthward-propagating dipolarization fronts, *Geophys. Res. Lett.*, 39,
352 <https://doi.org/10.1029/2012GL051784>, 2012.
- 353 Hasegawa, A., Drift mirror instability in the magnetosphere, *Phys. Fluids*, 12, 2642–
354 2650, 1969.
- 355 Huang, S. Y., Fu, H. S., Vaivads, A., Yuan, Z. G., Pang, Y., Zhou, M., Khotyaintsev,
356 Yuri V., Deng, X. H., André, M., Zhang, L., Fu, S., Li, H. M., and Wang, D. D.,
357 Dawn-dusk scale of dipolarization front in the earth's magnetotail: multi-cases study,
358 *Astrophys. Space Sci.*, 357, 1–7, <https://doi.org/10.1007/s10509-015-2298-3>, 2015.
- 359 Horbury, T. S., and Lucek, E. A., Size, shape, and orientation of magnetosheath mirror
360 mode structures, *J. Geophys. Res.*, 114, <https://doi.org/10.1029/2009JA014068>,
361 2009.
- 362 Ge, Y. S., McFadden, J. P., Raeder, J., Angelopoulos, V., Larson, D., and
363 Constantinescu, O. D., Case studies of mirror-mode structures observed by THEMIS
364 in the near-Earth tail during substorms, *J. Geophys. Res.*, 116,
365 <https://doi.org/10.1029/2010JA015546>, 2011.
- 366 Ge, Y. S., Zhou, X. Z., Liang, J., Raeder, J., Gilson, M. L., Donovan, E., Angelopoulos,
367 V., and Runov, A., Dipolarization fronts and associated auroral activities: 1.
368 Conjugate observations and perspectives from global MHD simulations, *J. Geophys.*
369 *Res.*, 117, <https://doi.org/10.1029/2012JA017676>, 2012.
- 370 Glassmeier, K., Motschmann, U., Mazelle, C., Neubauer, F., Sauer, K., Fuselier, S.,
371 and Acua, M., Mirror modes and fast magnetoacoustic waves near the magnetic
372 pileup boundary of comet P/Halley, *J. Geophys. Res.*, 98, 20,955–20,964,
373 <https://doi.org/10.1029/93JA02582>, 1993.
- 374 Kivelson, M. G., and Southwood, D. J., Mirror instability: 2. The mechanism of
375 nonlinear saturation, *J. Geophys. Res.*, 101, 17,365–17,371,
376 <https://doi.org/10.1029/96JA01407>, 1996.
- 377 Kuznetsov, E. A., Passot, T., and Sulem, P. L., Dynamical Model for Nonlinear Mirror
378 Modes near Threshold, *Phys. Rev. Lett.*, 98(23),



- 379 <https://doi.org/10.1103/PhysRevLett.98.235003>, 2007.
- 380 Li, H., Zhou, M., Deng, X., Yuan, Z., and Huang, S., Electron dynamics and wave
381 activities associated with mirror mode structures in the near-Earth magnetotail, *Sci.*
382 *China-Technol. Sci.*, 57(8), 1541–1551, <https://doi.org/10.1007/s11431-014-5574-5>,
383 2014.
- 384 Liu, J., Angelopoulos, V., Zhou, X. Z., Runov, A., and Yao, Z. H., On the role of
385 pressure and flow perturbations around dipolarizing flux bundles, *J. Geophys. Res.-*
386 *Space*, 118, 7104–7118, <https://doi.org/10.1002/2013JA019256>, 2013.
- 387 Pollock, C., Moore, T., Jacques, A., et al.: Fast plasma investigation for magnetospheric
388 multiscale, *Space Sci. Rev.*, 199, 331–406, 2016.
- 389 Rae, I. J., Mann, I. R., Watt, C. E. J., Kistler, L. M., and Baumjohann, W., Equator-S
390 observations of drift mirror mode waves in the dawnside magnetosphere, *J. Geophys.*
391 *Res.*, 112, <https://doi.org/10.1029/2006JA012064>, 2007.
- 392 Russell, C. T., Blanco - Cano, X., Jian, L. K., and Luhmann, J. G., Mirror - mode
393 storms: STEREO observations of protracted generation of small amplitude waves,
394 *Geophys. Res. Lett.*, 36, 2009.
- 395 Russell, C., Anderson, B., Baumjohann, W., Bromund, K., Dearborn, D., Fischer, D.,
396 Le, G., Leinweber, H., Leneman, D., Magnes, W., et al.: The magnetospheric
397 multiscale magnetometers, *Space Sci. Rev.*, 199, 189–256, 2016.
- 398 Schmid, D., Volwerk, M., Nakamura, R., Baumjohann, W., and Heyn, M., A statistical
399 and event study of magnetotail depolarization fronts, *Ann. Geophys.*, 29(9), 1537–
400 1547, <https://doi.org/10.5194/angeo-29-1537-2011>, 2011.
- 401 Schmid, D., Volwerk, M., Plaschke, F., Vörös, Z., Zhang, T. L., Baumjohann, W., and
402 Narita, Y., Mirror mode structures near Venus and Comet P/Halley, *Ann. Geophys.*,
403 32, 651–657, <https://doi.org/10.5194/angeo-32-651-2014>, 2014.
- 404 Schmid, D., Nakamura, R., Volwerk, M., Plaschke, F., Narita, Y., Baumjohann, W.,
405 Magnes, W., Fischer, D., Eichelberger, H. U., Torbert, R. B., Russell, C. T.,
406 Strangeway, R. J., Leinweber, H. K., Le, G., Bromund, K. R., Anderson, B. J., Slavin,
407 J. A., and Kepko, E. L., A comparative study of dipolarization fronts at MMS and
408 Cluster, *Geophys. Res. Lett.*, 43, 6012–6019, <https://doi.org/10.1002/2016GL069520>,
409 2016.
- 410 Sergeev, V., Runov, A., Baumjohann, W., Nakamura, R., Zhang, T. L., Volwerk, M.,
411 Balogh, A., Rème, H., Sauvaud, J. A., André, M., and Klecker, B., Current sheet
412 flapping motion and structure observed by Cluster, *Geophys. Res. Lett.*, 30(6), 1327,
413 [doi:10.1029/2002GL016500](https://doi.org/10.1029/2002GL016500), 2003.
- 414 Sonnerup, B. U. Ö., and Scheible, M., Minimum and maximum variance analysis, *ISSI*
415 *Sci. Rep. Ser.*, 1, 185–220, 1998.
- 416 Soucek, J., Lucek, E., and Dandouras, I., Properties of magnetosheath mirror modes
417 observed by Cluster and their response to changes in plasma parameters, *J. Geophys.*
418 *Res.*, 113, <https://doi.org/10.1029/2007JA012649>, 2008.
- 419 Southwood, D. J., and Kivelson, M. G., Mirror instability: 1. The physical mechanism
420 of linear instability, *J. Geophys. Res.*, 98, 9181–9187, 1993.
- 421 Tsurutani, B. T., Smith, E. J., Anderson, R. R., Ogilvie, K. W., Scudder, J. D., Baker,
422 D. N., and Bame, S. J., Lion roars and nonoscillatory drift mirror waves in the



- 423 magnetosheath, *J. Geophys. Res.*, **87**, 6060–6072,
424 <https://doi.org/10.1029/JA087iA08p06060>, 1982.
- 425 Tsurutani, B. T., Lakhina, G. S., Verkhoglyadova, O. P., Echer, E., Guarnieri, F. L.,
426 Narita, Y., and Constantinescu, D. O., Magnetosheath and heliosheath mirror mode
427 structures, interplanetary magnetic decreases, and linear magnetic decreases:
428 Differences and distinguishing features, *J. Geophys. Res.*, **116**,
429 <https://doi.org/10.1029/2010JA015913>, 2011.
- 430 Vaivads, A., Baumjohann, W., Haerendel, G., Nakamura, R., Kucharek, H., Klecker,
431 B., Lessard, M. R., Kistler, L. M., Mukai, T., and Nishida, A., Compressional Pc5
432 type pulsations in the morningside plasma sheet, *Ann. Geophys.*, **19**, 311–320,
433 <https://doi.org/10.5194/angeo-19-311-2001>, 2001.
- 434 Volwerk, M., Multi-satellite observations of ULF waves, in *Magnetospheric ULF*
435 *Waves: Synthesis and New Directions*, edited by K. Takahashi et al., pp. 109–135,
436 AGU, Washington, D. C., 2006.
- 437 Volwerk, M., Zhang, T. L., Delva, M., Vörös, Z., Baumjohann, W., and Glassmeier,
438 K.-H., Mirror-mode-like structures in Venus’ induced magnetosphere, *J. Geophys.*
439 *Res.*, **113**, <https://doi.org/10.1029/2008JE003154>, 2008.
- 440 Volwerk, M., Richter, I., Tsurutani, B., Götz, C., Altwegg, K., Broiles, T., Burch, J.,
441 Carr, C., Cupido, E., Delva, M., Dósa, M., Edberg, N. J. T., Eriksson, A., Henri, P.,
442 Koenders, C., Lebreton, J. P., Mandt, K. E., Nilsson, H., Opitz, A., Rubin, M.,
443 Schwingenschuh, K., Wieser, G. S., Szego, K., Vallat, C., Vallieres, X., Glassmeier,
444 K. H., Mass-loading, pile-up, and mirror-mode waves at comet 67P/Churyumov-
445 Gerasimenko, *Ann. Geophys.*, **34**, 1–15, <https://doi.org/10.5194/angeo-34-1-2016>,
446 2016.
- 447 Wang, G. Q., Volwerk, M., Nakamura, R., Boakes, P., Zhang, T. L., Yoshikawa, A., and
448 Baishev, D. G., Flapping current sheet with superposed waves seen in space and on
449 the ground, *J. Geophys. Res. Space Physics*, **119**,
450 <https://doi.org/10.1002/2014JA020526>, 2014.
- 451 Wang, G. Q., Zhang, T. L., Volwerk, M., Schmid, D., Baumjohann, W., Nakamura, R.,
452 and Pan, Z. H., Mirror mode structures ahead of dipolarization front near the neutral
453 sheet observed by Cluster, *Geophys. Res. Lett.*, **43**,
454 <https://doi.org/10.1002/2016GL070382>, 2016.
- 455 Wang, G. Q., Volwerk, M., Zhang, T. L., Schmid, D., and Yoshikawa, A., High-latitude
456 Pi2 pulsations associated with kink-like neutral sheet oscillations, *J. Geophys. Res.*
457 *Space Physics*, **122**, <https://doi.org/10.1002/2016JA023370>, 2017.
- 458 Wu, M. Y., Lu, Q. M., Volwerk, M., Vörös, Z., Zhang, T. L., Shan, L. C., and Huang,
459 C., A statistical study of electron acceleration behind the dipolarization fronts in the
460 magnetotail, *J. Geophys. Res. Space Physics*, **118**, 4804–4810,
461 <https://doi.org/10.1002/jgra.50456>, 2013.
- 462 Xiao, S. D., Zhang, T. L., Wang, G. Q., Volwerk, M., Ge, Y. S., Schmid, D., Nakamura,
463 R., Baumjohann, W., Plaschke, F., Occurrence rate of dipolarization fronts in the
464 plasma sheet: Cluster observations, *Ann. Geophys.*, **35**,
465 <https://doi.org/10.5194/angeo-35-1015-2017>, 2017.
- 466 Zhang, T. L., Russell, C. T., Baumjohann, W., Jian, L. K., Balikhin, M. A., Cao, J. B.,



- 467 Wang, C., Blanco-Cano, X., Glassmeier, K. H., Zambelli, W., Volwerk, M., Delva,
468 M., Vörös, Z., Characteristic size and shape of the mirror mode structures in the solar
469 wind at 0.72 AU, *Geophys. Res. Lett.*, 35, <https://doi.org/10.1029/2008GL033793>,
470 2008.
- 471 Zhang, T. L., Baumjohann, W., Russell, C. T., Jian, L. K., Wang, C., Cao, J. B.,
472 Balikhin, M., Blanco-Cano, X., Delva, M., and Volwerk, M., Mirror mode structures
473 in the solar wind at 0.72 AU, *J. Geophys. Res.*, 114,
474 <https://doi.org/10.1029/2009JA014103>, 2009.
- 475 Zhang, L., He, J. S., Zhao, J. S., Yao, S., and Feng, X. S., Nature of magnetic holes
476 above ion scales: a mixture of stable slow magnetosonic and unstable mirror modes
477 in a double - polytropic scenario?, *Astrophys. J.*, 864, 35.
478 <https://doi.org/10.3847/1538-4357/aad4aa>, 2018.
- 479 Zieger, B., Retinò, A., Nakamura, R., Baumjohann, W., Vaivads, A., and Khotyaintsev,
480 Y., Jet front-driven mirror modes and shocklets in the near-Earth flow-braking region,
481 *Geophys. Res. Lett.*, 38, <https://doi.org/10.1029/2011GL049746>, 2011.



482 **Author contribution**

483 Guoqiang Wang and Tielong Zhang designed the main idea of this study, and and the
484 data analysis was mainly performed by Guoqiang Wang. Guoqiang Wang prepared the
485 manuscript with contributions from all co-authors.

486

487 **Acknowledgements**

488 This work in China was supported by NSFC grants 41804157, 41774171, and
489 41974205. The authors also acknowledge the financial supported by the grant from Key
490 Laboratory of Lunar and Deep Space Exploration, CAS, Shenzhen Science and
491 Technology Research Program (JCYJ20170811154933612), and the 111 project
492 [B18017]. We acknowledge the data from the NASA MMS mission. We also
493 acknowledge MMS project FGM and FPI teams. The data of the MMS spacecraft are
494 publicly available at <https://lasp.colorado.edu/mms/sdc/public/>.

495

496 **Code/Data availability**

497 The data of the MMS spacecraft are publicly available at
498 <https://lasp.colorado.edu/mms/sdc/public/>.

499

500 **Competing interests**

501 The authors declare that they have no conflict of interest.